J Optim Theory Appl (2010) 144: 367–390
DOI 10.1007/s10957-009-9597-1

Synthesis of Optimal Control for Cooperative Collision Avoidance for Aircraft (Ships) with Unequal Turn Capabilities

T. Tarnopolskaya · N. Fulton

Published online: 28 August 2009

Abstract This paper presents a synthesis of an optimal control solution for cooperative collision avoidance strategies for aircraft (ships) with unequal turn capabilities in a close proximity coplanar encounter. The analytic expressions for the extremals are presented and their properties are analyzed. Simple algorithms for the synthesis of optimal control are developed. The structure of the synthesis is analyzed and its behavior with a change in the nondimensional turn rate ratio is studied. It is shown that Merz's solution for identical aircraft (see Merz in Proc. Joint Automatic Control Conf., Paper 15-3, pp. 449–454, 1973; Navigation 20(2):144–152, 1973; Tarnopolskaya and Fulton in J. Optim. Theory Appl. 140(2):355–375, 2009) is a degenerate case of this more general solution. The results of this paper are useful for benchmarking and validating automated proximity management and collision avoidance systems.

Keywords Collision avoidance · Cooperative maneuvers · Optimal control · Mayer problem · Pontryagin maximum principle · Unequal turn rates · Close proximity

1 Introduction

Both airborne and ground-based systems that provide aircraft proximity management functions are currently under intensive review. Programs such as Free Flight in the

Communicated by H.J. Pesch.

We thank the anonymous referees for helpful comments and suggestions.

T. Tarnopolskaya (✉)
CSIRO Mathematical & Information Sciences, Locked Bag 17, North Ryde, NSW 1670, Australia
e-mail: tanya.tarnopolskaya@csiro.au

N. Fulton
CSIRO Mathematical & Information Sciences, GPO Box 664, Canberra, ACT 2601, Australia
e-mail: neale.fulton@csiro.au

USA and Free Route in Europe will require at least some re-design and validation of these functions. This need is reinforced by an expected increase in the frequency of aircraft proximity incidents that will result from the growth in demand for air travel, and the introduction of aerial vehicle operations (without a human pilot) and personalized jets. Close proximity situations can occur, for example, in the missed approach, in the circuit area, and for operations outside controlled (managed) airspace where air traffic management (ATM) services may be unavailable and where aircraft routinely fly in closer proximity. Such situations require dependable proximity management at physical limits well below the more commonly understood ATM separation standards used in the present managed (controlled) airspace or those presently proposed for Free Flight airspace. The assurance of both miss distance and available response time during close proximity situations are important objectives [1, 2]. The maximization of terminal miss distance [3–8] remains an important and adequate objective for many close proximity conflict resolution situations for both aircraft and ships. Such a performance criterion is assumed in this paper.

Over the past two decades, a considerable advance has been made in the study of both the optimal resolution of ship conflicts [6, 7, 9] and of aircraft conflicts [8, 10–27]. While an advance in numerical optimization techniques makes it possible to study complex scenarios involving many participants, such solutions rely on complex computational techniques and on the correctness and convergence of calculations. It is therefore important that such results be validated against analytic or semi-analytic solutions. Synthesis of optimal control solutions for simplified scenarios are especially valuable as they allow the validation of an entire family of scenarios. Such solutions are the focus of this paper.

The coplanar close proximity encounter between two aircraft (ships) was first studied by Merz [3, 4], who presented the synthesis of the optimal control for identical aircraft (ships) in the form of 2D diagram. The Merz solution partitions the plane of the initial relative positions of the aircraft into two half-planes. In one half-plane, the relative distance is decreasing (converging). For the other half-plane, divergence (increase in relative distance) occurs. The convergence half-plane is further partitioned into three subplanes each corresponding to the initial conditions of a different optimal strategy. This diagram establishes the optimal collision avoidance strategy for both participants based on their initial relative position and orientation.

The rules by which aircraft avoid collisions are embedded in aviation law. These rules can be found in Annex 2 of [28]. In particular, para. 3.2.2.2 for *Approaching head-on* states: "When two aircraft are approaching head-on or approximately so and there is a danger of collision, each shall alter its heading to the right." Even a superficial examination of the Merz's solution [3–5] shows that this requirement will provide, in a significant number of situations, suboptimal outcomes for the proximity situation it is intended to govern. Thus, the importance of the synthesis of the optimal control solution for coplanar encounter first presented by Merz [3, 4] should not be under-estimated. To date, such a solution was available only for the case of aircraft (ships) of identical speed and turn capabilities [3–5]. The motivation behind this paper was to extend Merz's solution for the cases of nonidentical aircraft (ships).

This paper extends earlier analyses [3–5] to the case of aircraft with identical linear speeds but different turn capabilities. In practice, when two aircraft come into

proximity, their speeds are rarely equal. Nevertheless, there are a significant number of operational situations in which the aircraft linear speeds may be nearly equal. Such a confinement can arise from aircraft with similar types of power-plants (e.g., piston, turbo-propeller, turbo-jet, etc.) performing similar operations (climb, descent, cruising flight, etc.), or dissimilar aircraft types performing prescribed procedures (e.g., missed approach, instrument approaches, speed restrictions, etc.). In these cases, speed differentials can be very small and the results of this paper will be broadly applicable. At the same time, the maximum turn rates can be significantly different (this is discussed in more detail in Sect. 2).

An assumption of a coplanar encounter adopted in this and earlier studies is a natural one for ship collision avoidance. For aircraft, the coplanar assumption can cover those situations where both aircraft are maneuvering at the same constant altitude or when they maneuver with individually small flight-path angles measured with respect to a shared earth tangential plane. In this latter case the solution presented in this paper can be applied to the projected ground tracks of the aircraft involved.

The aim of this paper is to derive a benchmark (ideal solution) against which practical solutions as well as automatic collision avoidance systems can be assessed. For this reason, and for the purpose of this paper, we assume that perfect information about the relative position and individual velocity vectors of the participants is available. In practice, state information is inaccurate due to measurement noise and the overall system performance will be measured by performance metrics such as required navigation performance (RNP). The resulting system level errors will differ considerably for each aircraft dependent on the characteristics of the type of navigation system (e.g., GPS, Inertial Navigation System, etc.) fitted to the aircraft. For example, if the proximity pair is composed of two aircraft each equipped with GPS, the error in relative position of the participants will be negligible. If one aircraft is equipped with a GPS and another with an INS, then a differential error can arise. Thus, the stochastic formulation would need to be specific to the combination of navigation systems used.

Existing airborne collision avoidance systems (ACAS)—e.g., TCAS II—resolve conflict in the vertical: one aircraft is commanded to climb, the other to descend. Limiting ACAS systems to only vertical maneuvers can over restrict a pilot's options to resolve the conflict and can in some circumstance lead to additional danger (e.g., in the presence of terrain, if commanded to ascend into a layer of cloud which will form ice, etc.). For these reasons new collision avoidance systems (e.g., TCAS IV) are also considering lateral maneuvers. The optimal maneuver in a particular operational circumstance may be a composite of both vertical and lateral maneuvers. This paper forms a foundational work required for the verification and validation of the lateral component of the maneuver.

The analysis in this paper is based on the Pontryagin maximum principle [29–31] for a Mayer problem. The analytic solutions for the extremals are presented and their properties are analysed. The synthesis of optimal control is constructed based on the analysis of the properties of the extremals. The analysis shows that the structure of the optimal control solution for aircraft (ships) with unequal turn rates is significantly more complex than in the case of identical aircraft (ships). Thus, Merz' solution for identical aircraft (ships) [3–5] represents a degenerate case of this more general solution.

In what follows, the terminology common in aviation is used. However, the analysis is equally applicable to ship collision avoidance and robotics.

2 Equations of Motion

Consider two aircraft flying at the same altitude with equal linear speed but different turn capabilities. One of the aircraft (which we will call the first aircraft for definiteness) is placed at the origin of the moving coordinate system in such a way that its velocity vector coincides with the direction of the y-axis (Fig. 1). The nondimensional equations of motion in the moving polar coordinate system are [3–5]

$$\begin{aligned} \dot{r}^* &= -\cos\phi + \cos(\theta - \phi), \\ \dot{\phi} &= -\sigma_1 + [\sin\phi + \sin(\theta - \phi)]/r^*, \\ \dot{\theta} &= -\sigma_1 + \omega\sigma_2, \end{aligned} \tag{1}$$

where $r^* = r/R_{1,\min}$, r is the instantaneous relative position of the aircraft, ϕ and θ are the instantaneous angles defining the relative orientation of the aircraft (Fig. 1); σ_1 and σ_2 are the nondimensional angular speeds of aircraft $\sigma_1 = \omega_1/|\omega_{1,\max}|$, $\sigma_2 = \omega_2/|\omega_{2,\max}|$; ω_1 and ω_2 are the angular speeds, with positive values corresponding to the right turns (a clockwise turn in the earth tangential plane when viewed from above), and negative values corresponding to the left turns (therefore $|\sigma_1| \le 1$, $|\sigma_2| \le 1$); $\omega_{1,\max}$ and $\omega_{2,\max}$ are maximum turn rates of the first and second aircraft respectively, while $R_{1,\min}$ is the minimum turn radius of the first aircraft; ω is the nondimensional parameter which represents the ratio of the absolute values of maximum turn rates $\omega = |\omega_{2,\max}|/|\omega_{1,\max}| > 0$. The angle ϕ is known as a relative bearing in aircraft navigation and is measured in clockwise direction from the y-axis, while the angle θ is known as a relative heading (Fig. 1). The dots denote the derivatives with respect to nondimensional time $t^* = t|\omega_{1,\max}|$. In the Cartesian coordinate sys-

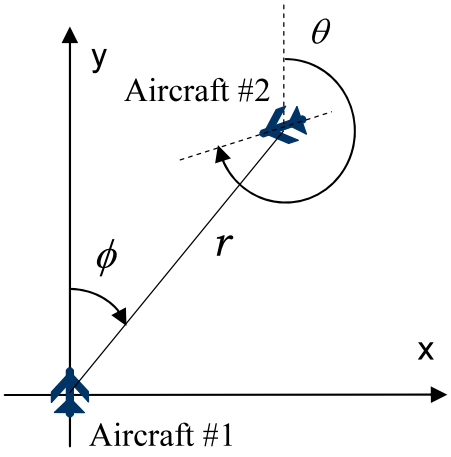

Fig. 1 Schematics of the coplanar encounter in the moving coordinate system

tem, the nondimensional equations of motion are

$$\dot{x}^* = -\sigma_1 y^* + \sin\theta, \qquad \dot{y}^* = -1 + \sigma_1 x^* + \cos\theta, \qquad \dot{\theta} = -\sigma_1 + \omega\sigma_2, \tag{2}$$

where $x^* = x/R_{1,\min}$, $y^* = y/R_{1,\min}$, and x, y are the Cartesian coordinates of the second aircraft relative to the first one. Note that $r^* = \sqrt{x^{*2} + y^{*2}}$, $\sin\phi = x^*/r^*$, $\cos\phi = y^*/r^*$.

For the sake of definiteness, the relative heading and relative bearing are defined as

$$0 \le \theta < 2\pi, \qquad -\pi \le \phi < \pi. \tag{3}$$

In what follows, we consider the nondimensional quantities only and omit the superscript stars for simplicity.

The important subclass of the problem for aircraft (ships) of identical speed and turn capabilities ($\omega = 1$) was first studied by Merz [3, 4], and a rigorous analysis is presented in [5]. This paper extends the earlier analyses to the case of aircraft with different turn capabilities (that is, $\omega > 0$). The turn rates for individual aircraft can vary significantly from zero to over 90 degrees/second. Since it is assumed that the aircraft have equal speeds, the ratio of maximum turn rates ω falls in the interval $[1/R^*, R^*]$, where R^* is the ratio of minimum turn radii. The minimum turn radius depends on: the aircraft configuration (position of the flaps and the landing gear); limitations imposed on the angle of bank (e.g., 60 degrees is common) by the design; and on the true airspeed at the time of banking. Broad consideration of these factors would suggest that ω will typically fall in the interval $(0.1, 10)$.

3 Optimization Problem

In the polar coordinate system, the system of ordinary differential equations (1) can be considered as a control system with state vector $\rho^T = (r, \phi, \theta)$ and control function $u^T = (\sigma_1, \sigma_2)$, $u : [0, T] \to U$, $U \subseteq R^2$, $U = [-1, 1] \times [-1, 1]$,

$$\begin{aligned} &\dot{\rho} = f_p(\rho, u) \\ &\quad = \big[-\cos\phi + \cos(\theta - \phi), \quad -\sigma_1 + [\sin\phi + \sin(\theta - \phi)]/r, \quad -\sigma_1 + \omega\sigma_2\big]^T, \\ &\rho|_{t=0} = \rho_0. \end{aligned} \tag{4}$$

In Cartesian coordinates, the state vector is $X^T = (x, y, \theta)$ and (2) can be written as

$$\begin{aligned} &\dot{X} = f(X, u) = \big[-\sigma_1 y + \sin\theta, \quad -1 + \sigma_1 x + \cos\theta, \quad -\sigma_1 + \omega\sigma_2\big]^T, \\ &X|_{t=0} = X_0. \end{aligned} \tag{5}$$

The time of the maneuver T (also known as a terminal time) is defined as the time of closest approach between the two aircraft. It is defined by the conditions

$$\dot{r}(T) = 0, \quad \dot{r}(t) < 0, \quad t \in [0, T). \tag{6}$$

The objective is to maximize the terminal miss distance $\psi(T,u)$ over all admissible controls

$$\max_{u\in U}[\psi(T,u)]. \tag{7}$$

Thus, the performance index is a function of terminal time only. As the terminal time T is unknown, the problem can be considered as a Mayer problem with free terminal point [29–31]. In polar coordinates, the performance index is given by $\psi(\rho(T,u)) = r|_{t=T} \equiv r_T$, while in Cartesian coordinates it is $\psi(X(T,u)) = \sqrt{x^2|_{t=T} + y^2|_{t=T}}$.

4 Necessary Conditions for Nonsingular Optimal Control

We define the Hamiltonian function in the polar coordinate system as follows:

$$\begin{aligned} H(\lambda(t),\rho(t),u(t)) &= \lambda_P^T \cdot f_p(\rho,u) \\ &= \lambda_r(t)\dot{r}(t,u) + \lambda_\phi(t)\dot{\phi}(t,u) + \lambda_\theta(t)\dot{\theta}(t,u) \\ &= \lambda_r[-\cos\phi + \cos(\theta-\phi)] \\ &\quad + \lambda_\phi\{-\sigma_1 + [\sin\phi + \sin(\theta-\phi)]/r\} \\ &\quad + \lambda_\theta(-\sigma_1 + \omega\sigma_2), \end{aligned} \tag{8}$$

where the adjoint variables $\lambda_P^T(t) \equiv (\lambda_r(t), \lambda_\phi(t), \lambda_\theta(t))$ satisfy the equations

$$\dot{\lambda}_P = -\nabla H = \begin{bmatrix} \lambda_\phi[\sin\phi + \sin(\theta-\phi)]/r^2 \\ -\lambda_r(\sin\phi + \sin(\theta-\phi)) - \lambda_\phi[\cos\phi - \cos(\theta-\phi)]/r \\ \lambda_r\sin(\theta-\phi) + \lambda_\phi\cos(\theta-\phi)/r \end{bmatrix},$$

$$\lambda_P(T) = \nabla\psi(\rho(T)) = [1,0,0]^T. \tag{9}$$

The transversality condition is given by

$$\dot{\psi}|_{t=T} \equiv \left.\frac{\partial\psi}{\partial t}\right|_{t=T} + \nabla\psi\cdot\dot{\rho}|_{t=T} = \dot{r}|_{t=T} = 0.$$

The Pontryagin maximum principle [29–31] states that, in order that $\hat{u}(t)$ and $\hat{\rho}(t)$ be the optimal control and the optimal trajectory respectively for the Mayer problem with a free terminal point (4), (7), it is necessary that there exist a nonzero continuous vector function $\lambda_P(t)$ that satisfies (9) so that, for every $t\in[0,T]$, the following maximality condition holds:

$$H(\lambda_P(t),\hat{\rho}(t),\hat{u}(t)) = \max_{u\in U}\{H(\lambda_P(t),\hat{\rho}(t),u)\}. \tag{10}$$

4.1 Terminal Conditions

Consider now the first of terminal conditions (6) together with the first of (4), which give

$$\dot{r}(T) = \cos(\theta_T - \phi_T) - \cos\phi_T = 2\sin(\theta_T/2)\sin(\phi_T - \theta_T/2) = 0. \tag{11}$$

Equation (11) yields two possible terminal conditions: (1) $\theta_T/2 = \pi n$, $n = 0, \pm 1$, $\pm 2, \ldots$; (2) $\phi_T - \theta_T/2 = \pi k$, $k = 0, \pm 1, \pm 2$. Within the domain defined by conditions (3), these conditions reduce to

$$\theta_T = 0, \tag{12}$$

$$\phi_T = \theta_T/2 - \pi, \qquad \phi_T = \theta_T/2. \tag{13}$$

4.2 Necessary Conditions for Optimal Control in the Vicinity of Terminal Time

The maximality condition (10) can be rewritten in the form

$$\begin{aligned} H(\lambda_P(t), \hat{\rho}(t), \hat{u}(t)) = {} & \max_{\sigma_1 \in [-1,1]} [\sigma_1(-\lambda_\phi - \lambda_\theta)] + \max_{\sigma_2 \in [-1,1]} (\sigma_2 \omega \lambda_\theta) \\ & + \lambda_r[-\cos\phi + \cos(\theta - \phi)] \\ & + \lambda_\phi\{[\sin\phi + \sin(\theta - \phi)]/r\}. \end{aligned} \tag{14}$$

The two switching functions are given by $\Phi_1^{(p)} = \lambda_\phi + \lambda_\theta$, $\Phi_2^{(p)} = \omega\lambda_\theta$. In this section, we consider the case $\Phi_1^{(p)} \neq 0$, $\Phi_2^{(p)} \neq 0$. The possibility of singular arcs will be considered in Sect. 5.6.

It can be shown [5] that the terminal condition (12) together with (9) yields $\sigma_1 = -\sigma_2 = \pm 1$, that is, the aircraft are turning with maximum angular speed in opposite directions. We will call these strategies right-left (RL) and left-right (LR) strategies. The terminal condition (13) and (9) result in $\sigma_1 = \sigma_2 = \pm 1$, therefore both aircraft are turning with the maximum angular speed in the same directional sense. Such strategies will be called right-right (RR) and left-left (LL) strategies.

4.3 Extremals

In this section, the state equations (5) in terms of backward derivatives,

$$\mathring{x} = \sigma_1 y - \sin\theta, \qquad \mathring{y} = 1 - \sigma_1 x - \cos\theta, \qquad \mathring{\theta} = \sigma_1 - \omega\sigma_2 \tag{15}$$

are solved subject to the boundary conditions $x|_{\tau=0} = x_T$, $y|_{\tau=0} = y_T$, and one of the two terminal conditions (12), (13). Below, we consider the terminal conditions (12) and (13) separately.

Case I $\theta|_T = 0$, $\sigma_1 = -\sigma_2 = \pm 1$. This case corresponds to the RL and LR strategies. In this case, the solution of (15) is given by (taking into account the periodicity property of the angle θ, that is $\theta + 2\pi k = \theta$, $k = 0, \pm 1, \pm 2, \ldots$)

$$\begin{aligned} \theta &= \begin{cases} \sigma_1(1+\omega)\tau, & \sigma_1 = 1, \\ 2\pi + \sigma_1(1+\omega)\tau, & \sigma_1 = -1, \end{cases} \\ x &= r_T \sin(\phi_T + \sigma_1\tau) + \sigma_1[1 + \cos[(1+\omega)\tau]/\omega - (1+\omega)\cos\tau/\omega], \\ y &= r_T \cos(\phi_T + \sigma_1\tau) + (1+\omega)\sin\tau/\omega - \sin[(1+\omega)\tau]/\omega. \end{aligned} \tag{16}$$

For $\tau = T$, (16) give the initial conditions for the state variables

$$\begin{aligned}
\theta_0 &= \begin{cases} \sigma_1(1+\omega)T, & \sigma_1 = 1, \\ 2\pi + \sigma_1(1+\omega)T, & \sigma_1 = -1, \end{cases} \\
x_0 &= r_T \sin(\phi_T + \sigma_1 T) + \sigma_1\{1 + \cos[(1+\omega)T]/\omega - (1+\omega)\cos T/\omega\}, \\
y_0 &= r_T \cos(\phi_T + \sigma_1 T) + (1+\omega)\sin T/\omega - \sin[(1+\omega)T]/\omega. \qquad (17)
\end{aligned}$$

Equations (17) can be rewritten in the following form:

$$\begin{aligned}
\text{For } \sigma_1 = 1: \quad & \{x_0 - 1 - \cos\theta_0/\omega + (1+\omega)\cos[\theta_0/(1+\omega)]/\omega\}^2 \\
& + \{y_0 - (1+\omega)\sin[\theta_0/(1+\omega)]/\omega + \sin\theta_0/\omega\}^2 = r_T^2. \qquad (18) \\
\text{For } \sigma_1 = -1: \quad & \{x_0 + 1 + \cos\theta_0/\omega - (1+\omega)\cos[(\theta_0 - 2\pi)/(1+\omega)]/\omega\}^2 \\
& + \{y_0 + (1+\omega)\sin[(\theta_0 - 2\pi)/(1+\omega)]/\omega - \sin\theta_0/\omega\}^2 = r_T^2. \qquad (19)
\end{aligned}$$

Case II $\theta_T = 2\phi_T + 2\pi$ or $\theta_T = 2\phi_T$; $\sigma_1 = \sigma_2 = \pm 1$. This case corresponds to the RR and LL strategies. In this case, the solution of (15) takes the form

$$\begin{aligned}
\theta &= \sigma_1(1-\omega)\tau + \theta_T, \\
y &= r_T \cos(\phi_T + \sigma_1\tau) + \sin\tau \\
&\quad - \sigma_1\{\sin(\theta_T + \sigma_1\tau) - \sin[\theta_T + \sigma_1(1-\omega)\tau]\}/\omega, \\
x &= r_T \sin(\phi_T + \sigma_1\tau) + \sigma_1\cos(\theta_T + \sigma_1\tau)/\omega \\
&\quad + \sigma_1(1 - \cos\tau) - \sigma_1\cos[\theta_T + \sigma_1(1-\omega)\tau]/\omega. \qquad (20)
\end{aligned}$$

For $\tau = T$, we have $\theta_0 = \sigma_1(1-\omega)T + \theta_T$, and the two branches of the initial conditions for the state variables are given by

$$\begin{aligned}
x_0 &= r_T \sin[(\theta_0 + \sigma_1\omega T + \sigma_1 T)/2] \\
&\quad + \sigma_1[\cos(\theta_0 + \sigma_1\omega T) - \cos\theta_0]/\omega + \sigma_1(1 - \cos T), \\
y_0 &= r_T \cos[(\theta_0 + \sigma_1\omega T + \sigma_1 T)/2] + \sin T \\
&\quad - \sigma_1\sin(\theta_0 + \sigma_1\omega T)/\omega + \sigma_1\sin\theta_0/\omega, \qquad (21)
\end{aligned}$$

for $\phi_T = \theta_T/2$, and

$$\begin{aligned}
x_0 &= -r_T \sin[(\theta_0 + \sigma_1\omega T + \sigma_1 T)/2] \\
&\quad + \sigma_1[\cos(\theta_0 + \sigma_1\omega T) - \cos\theta_0]/\omega + \sigma_1(1 - \cos T), \\
y_0 &= -r_T \cos[(\theta_0 + \sigma_1\omega T + \sigma_1 T)/2] + \sin T \\
&\quad - \sigma_1\sin(\theta_0 + \sigma_1\omega T)/\omega + \sigma_1\sin\theta_0/\omega, \qquad (22)
\end{aligned}$$

for $\phi_T = \theta_T/2 - \pi$.

Equations (21)–(22) can be also written in the following form:

$$\begin{aligned}&[x_0-\sigma_1(1-\cos\theta_0/\omega)]^2+(y_0-\sigma_1\sin\theta_0/\omega)^2\\&\quad=r_T^2+2-2\cos[\theta_0-\sigma_1(1-\omega)T]/\omega\\&\qquad-2r_T\sigma_1(1+1/\omega)\sin[(\theta_0-\sigma_1(1-\omega)T)/2],\end{aligned}\tag{23}$$

for $\phi_T=\theta_T/2$, and

$$\begin{aligned}&[x_0-\sigma_1(1-\cos\theta_0/\omega)]^2+(y_0-\sigma_1\sin\theta_0/\omega)^2\\&\quad=r_T^2+2-2\cos[\theta_0-\sigma_1(1-\omega)T]/\omega\\&\qquad+2r_T\sigma_1(1+1/\omega)\sin[(\theta_0-\sigma_1(1-\omega)T)/2],\end{aligned}\tag{24}$$

for $\phi_T=\theta_T/2-\pi$.

5 Optimal Air Collision Avoidance Strategy

This section presents a justification for the optimal collision avoidance strategies and for the construction of the synthesis of optimal control. We start by establishing several properties of the extremals that will be useful for subsequent analysis.

5.1 Properties of Extremals

Property 5.1 *The loci of the initial conditions for the RL and LR strategies represent circles. The centers of the loci of initial conditions for the RL strategy* (18) *lie on the line that goes through the origin and forms the angle η_1 with the vertical axis so that*

$$\begin{aligned}\tan\eta_1=&\big\{\omega+\cos\theta_0-(\omega+1)\cos[\theta_0/(1+\omega)]\big\}\\&/\big\{(\omega+1)\sin[\theta_0/(1+\omega)]-\sin\theta_0\big\},\end{aligned}\tag{25}$$

while the centers of the loci of initial conditions for the LR strategy (19) *lie on the line that goes through the origin and forms the angle η_2 with the vertical axis*,

$$\begin{aligned}\tan\eta_2=&\big\{-\omega-\cos\theta_0+(\omega+1)\cos[(\theta_0-2\pi)/(1+\omega)]\big\}\\&/\big\{-(\omega+1)\sin[(\theta_0-2\pi)/(1+\omega)]+\sin\theta_0\big\}.\end{aligned}\tag{26}$$

For $\omega=1$ (Merz' solution for identical aircraft [3–5]*), the centers of these loci lie on the same line that goes through the origin and forms the angle $\eta=\theta_0/2-\pi/2$ with the vertical axis.*

Proof This follows immediately from (18) and (19). □

Property 5.2 *The following properties hold for the loci of the initial positions for the RL and LR strategies for a given r_T:*

(1) *The radial coordinates of the centers of loci of the LR strategies are larger than the radial coordinates of the centers of loci of the RL strategies for* $0 < \theta_0 < \pi$, *and smaller for* $\pi < \theta_0 < 2\pi$.
(2) *For* $\theta_0 = \pi$, *the loci of the initial positions for the RL and LR strategies are symmetric about the y-axis, and their radial coordinates coincide.*

Proof Indeed, for $\theta_0 = \pi$, we have $x^c_{RL} = -x^c_{LR} = 1 - 1/\omega - (1+\omega)\cos[\pi/(1+\omega)]/\omega$; $y^c_{RL} = y^c_{LR} = (1+\omega)\sin[\pi/(1+\omega)]/\omega$, and therefore the loci are symmetric relative to y-axis and $R^c_{RL} = R^c_{LR}$. For the general case $0 \le \theta_0 \le 2\pi$, it is straightforward to show that $R^{c2}_{RL} - R^{c2}_{LR} = A\{\sin[\theta_0(1+\omega) - \pi/(1+\omega)] - \sin[\theta_0 - \theta_0(1+\omega) + \pi/(1+\omega)]/\omega\}$, where $A = 4(1+\omega)\sin[\pi/(1+\omega)]/\omega > 0$. By taking $\theta_0 = \pi + \varepsilon$, where ε is small, and expanding in small parameter ε yields $R^{c2}_{RL} - R^{c2}_{LR} \approx 2A\varepsilon/(1+\omega)$, and therefore $R^c_{RL} > R^c_{LR}$ for $\varepsilon > 0$ ($\theta_0 > \pi$) and $R^c_{RL} < R^c_{LR}$ for $\varepsilon < 0$ ($\theta_0 < \pi$). These results hold for any ε, as the function $R^{c2}_{RL} - R^{c2}_{LR}$ is monotonic. Indeed, it is straightforward to show that $\partial(R^{c2}_{RL} - R^{c2}_{LR})/\partial\theta_0 = 2A\sin(\theta_0/2)\sin[\theta_0 - \theta_0/(1+\omega) + \pi/(1+\omega)]/(1+\omega) \ge 0$ for $\forall\omega > 0$, $0 \le \theta_0 \le 2\pi$. □

Property 5.3 *The loci of the initial conditions for the RR and LL strategies*, (21), (22) (*or* (23), (24)) *for a given* θ_0 *and* r_T *and varying time of encounter,* T, *represent spirals with the centers at* $(\sigma_1(1 - \cos\theta_0/\omega), \sigma_1 \sin\theta_0/\omega)$. *The following properties hold*:

(1) *For* $\omega = 1$ (*Merz' solution for identical aircraft* [3–5]), *the spirals turn into circles with centers lying on the line passing through the origin and forming the angle* $\theta_0/2$ *with the vertical axis* (*counting clockwise from positive direction of y-axis*).
(2) *For* $\omega > 1$, *the spirals are bounded and contained between two concentric circles*; *As* $\omega \to \infty$, *the coordinates of the centers of spirals approach the points* $(\sigma_1, 0)$, *while the radii of the concentric circles bounding the spirals approach the values* $R_{small} = r_T^2 + 2 - 2r_T$; $R_{large} = r_T^2 + 2 + 2r_T$.
(3) *For* $\omega < 1$, *both the centers and the radii of the RR and LL spirals are unbounded and expanding as* $\omega \to 0$.

Proof The proof follows immediately from (23), (24). □

The behavior of the spirals with a change in ω is illustrated in Fig. 2.

5.2 Optimal Trajectories

In order to select the optimal trajectories from the set of extremals, one should:

(1) select the trajectories such that the relative distance between the aircraft (called a range in aviation) decreases on $t \in [0, T]$;
(2) among such trajectories, select those that maximize the terminal miss distance.

Firstly, consider the trajectories along which the relative distance (range) decreases, that is $\dot r = 2\sin(\theta/2)\sin(\phi - \theta/2) < 0$, $t \in [0, T)$. This inequality yields, for the rela-

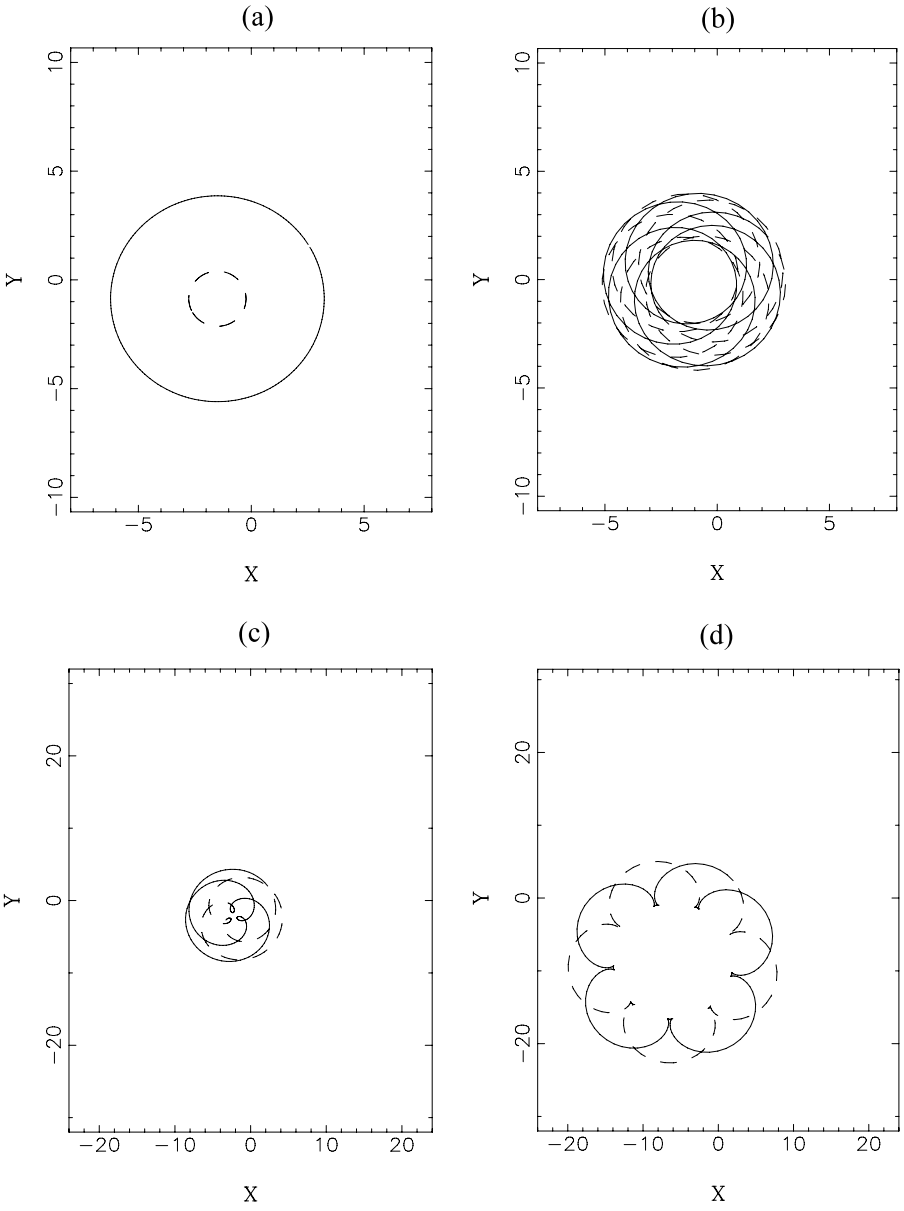

Fig. 2 Transformation of the loci of initial conditions for LL strategies with change in ω; $\theta_0 = 2\pi/3$, $r_T = 3$; Loci corresponding to branches $\phi_T = \theta_T/2$ and $\phi_T = \theta_T/2 - \pi$ are shown with *solid and dashed lines* respectively; (**a**) $\omega = 1$; (**b**) $\omega = 10$; (**c**) $\omega = 0.4$; (**d**) $\omega = 0.1$

tive bearing defined by (3): $\theta/2 - \pi < \phi < \theta/2$, $t \in [0, T)$. For $t = 0$, this inequality reduces to

$$\theta_0/2 - \pi < \phi_0 < \theta_0/2. \tag{27}$$

Thus, the straight line

$$\tan\phi = \tan(\theta_0/2) \tag{28}$$

divides the plane of the initial relative positions of the aircraft into the two subplanes of initial relative positions for the trajectories with positive and negative initial range rate. We will call this line an initial zero range rate line.

The trajectories that start on the loci of the initial conditions for the RR or LL strategies (21), (22) end, for a given θ_0 and T, on the line

$$\tan\phi|_{t=T} = \tan\{[\theta_0 - \sigma_1(1-\omega)T]/2\}. \tag{29}$$

We call this line a terminal zero range rate line. The following Properties follow immediately from (29):

Property 5.4 *The initial and the terminal zero range rate lines for RR and LL strategies coincide for two cases*:

(1) $\omega = 1$;
(2) *in the limit* $T \to 0$.

Property 5.5 *For* $\omega > 1$, *the terminal zero range rate line moves anticlockwise relative to the initial zero range rate line with increase in the encounter time* T *for* $\sigma_1 = -1$ *and clockwise for* $\sigma_1 = 1$. *For* $\omega < 1$, *the terminal zero range rate line moves anticlockwise relative to the initial zero range rate line with increase in the encounter time* T *for* $\sigma_1 = 1$ *and clockwise for* $\sigma_1 = -1$ (*see Fig.* 3).

We now consider the part of the loci of initial conditions with $T \in [0, T^*]$, where the time of encounter T is relatively small for close proximity situations. It is useful to note that the loci of initial conditions for the RR and LL strategies (23), (24) can be separated into the two families: the loci with larger and smaller radii. Thus, the loci (23) with $\sigma_1 = -1$ and the loci (24) with $\sigma_1 = 1$ belong to the family of loci with larger radii. Numerical analysis shows that the loci with smaller radii correspond to suboptimal strategies. Three situations are possible for such loci:

(1) The point on the loci does not satisfy (27).
(2) The point on the loci satisfies (27), but condition $\dot{r} < 0$ on $t \in [0, T)$ is not satisfied.
(3) Conditions (27) and $\dot{r} < 0$ on $t \in [0, T)$ are satisfied, but the point does not belong to the internal envelope discussed further in this section.

In what follows, we consider only the family of the RR and LL loci with larger radii. The properties of such loci can be summarized as follows.

Property 5.6 *For loci of initial relative positions for the RR strategy* (24) *and the LL strategy* (23), *the direction of motion of the trajectories that start on such loci is clockwise toward* $\phi_T = \theta_T/2$ *for strategy* $\sigma_1 = -1$ *and is anticlockwise toward* $\phi_T = \theta_T/2 - \pi$ *for* $\sigma_1 = 1$. *For such trajectories, there exists an interval* $T \in [0, \varepsilon]$, $\varepsilon > 0$, *such that the corresponding trajectories have decreasing relative distance* (*range*).

The trajectories with decreasing range are illustrated in Fig. 3 for the RR, LL and RL strategies. The instantaneous zero range rate line continuously changes for all optimal strategies. For given θ_0 and T, the RR and LL trajectories end on the corresponding terminal zero range rate line (see Figs. 3a and 3b). For the RL strategies, θ decreases towards zero along the trajectory and the trajectories end on the circle centered at the origin with the radius $r = r_T$, as illustrated in Fig. 3c.

We now consider, for given r_T and θ_0, the loci of the initial relative positions with associated strategies that deliver a given terminal miss-distance and ensure a decreasing range (relative distance) during the maneuver and denote it by $R(r_T, \theta_0, \omega) \equiv \{x_0, y_0, u : r|_{t=T} = r_T, \theta|_{t=0} = \theta_0\}$. We also define the internal envelope $\Re(r_T, \theta_0, \omega)$ of the relative positions with associated strategies $R(r_T, \theta_0, \omega)$ as

$$\Re(r_T, \theta_0, \omega) \equiv \Big\{(x_0^*, y_0^*, u) : (x_0^*, y_0^*, u) \in R(r_T, \theta_0, \omega) \quad \text{for } \forall \phi, r_\phi(x_0^*, y_0^*) = \min_{(x_0, y_0) \in R(r_T, \theta_0, \omega)} r_\phi(x_0, y_0)\Big\}.$$

Consider the loci of initial positions for the trajectories with decreasing range defined above. Denote the point of intersection of the RR loci (24) and the LL loci (23) in polar coordinates by $\mathbf{r}^{(0)}(r_T, \theta_0) = (r^{(0)}(r_T, \theta_0), \phi^{(0)}(r_T, \theta_0))$. Also denote the point of intersection of the RR loci (24) and RL (LR) loci by $\mathbf{r}^{(1)}(r_T, \theta_0) = (r^{(1)}(r_T, \theta_0), \phi^{(1)}(r_T, \theta_0))$. The point of intersection of the LL loci (23) and the RL (LR) loci is denoted by $\mathbf{r}^{(2)}(r_T, \theta_0) = (r^{(2)}(r_T, \theta_0), \phi^{(2)}(r_T, \theta_0))$. It follows from Property 5.2 that only the RL loci (18), for $0 < \theta_0 < \pi$, and only the LR loci (19), for $\pi < \theta_0 < 2\pi$, can belong to the internal envelope. Thus, the internal envelope $\Re(r_T, \theta_0, \omega)$ is given by:

$$\Re(r_T, \theta_0, \omega) = \begin{cases} \text{if } r^{(0)} \le r^{(1)}, & \text{arc of RR loci (24) for } \theta_0/2 - \pi < \phi < \phi^{(0)}, \\ & \text{arc of LL loci (23) for } \phi^{(0)} < \phi < \theta_0/2, \\ \text{if } r^{(0)} > r^{(1)}, & \text{arc of RR loci (24) for } \theta_0/2 - \pi < \phi < \phi^{(1)}, \\ & \text{arc of RL loci (18) for } \phi^{(1)} < \phi < \phi^{(2)}, 0 < \theta_0 < \pi, \\ & \text{arc of LR loci (19) for } \phi^{(1)} < \phi < \phi^{(2)}, \pi < \theta_0 < 2\pi, \\ & \text{arc of LL loci (23) for } \phi^{(2)} < \phi < \theta_0/2. \end{cases} \tag{30}$$

We can now prove the following result.

Lemma 5.1 *For each point (x_0, y_0) on the loci of relative positions with associated strategies $R(r_T, \theta_0, \omega)$ that lies outside the internal envelope $\Re(r_T, \theta_0, \omega)$, there exists an alternative strategy that delivers a terminal miss distance larger than r_T.*

Proof This follows from the fact that the radii of the RR, LL and RL loci are continuous increasing functions of r_T, while the coordinates of the centers of these loci are independent of r_T and fixed for a given θ_0. □

Corollary 5.1 *The strategies associated with the points on the loci $\Re(r_T, \theta_0, \omega)$ are the optimal strategies for given initial relative positions, r_T, θ_0 and ω.*

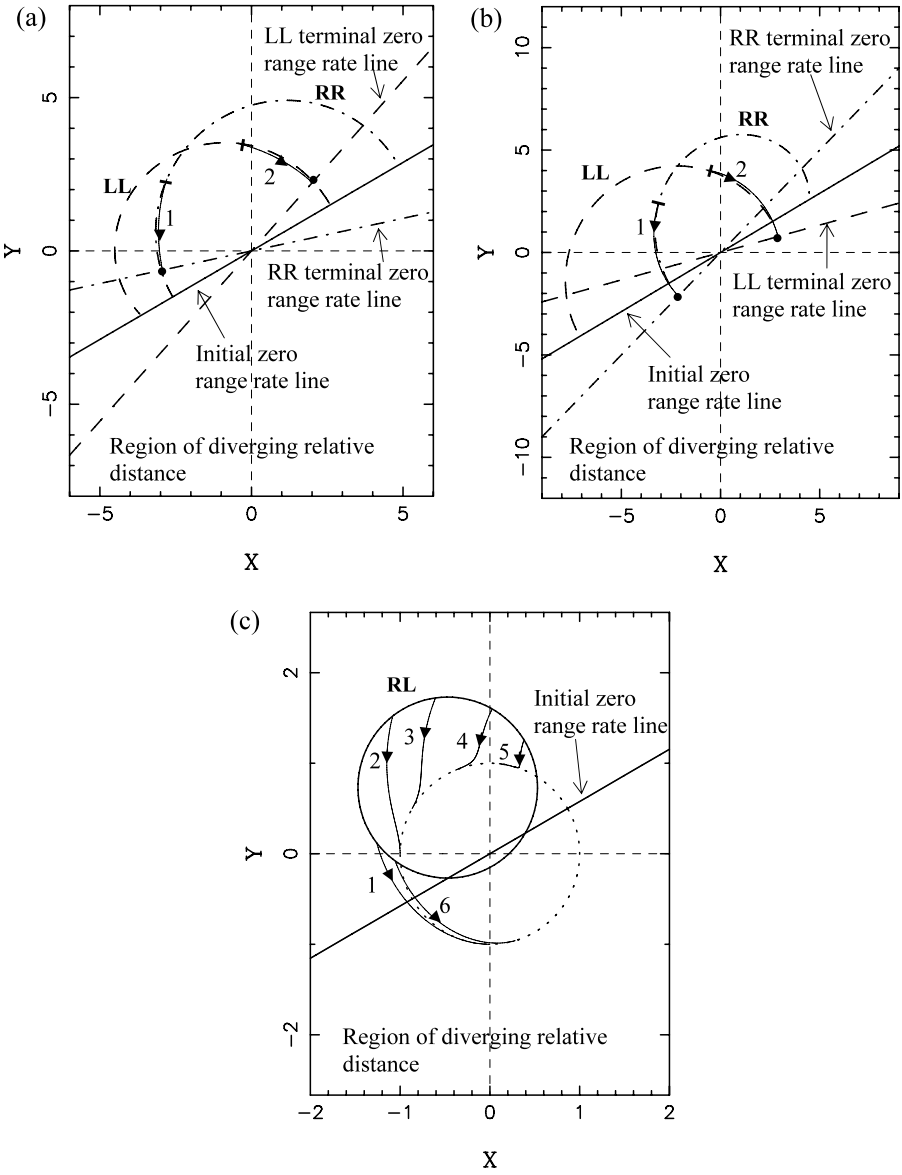

Fig. 3 Loci of the initial relative positions and trajectories for $\theta_0 = 2\pi/3$. *Figures 3a* and *3b* show such loci and trajectories for RR and LL strategies for $\omega = 2$ and $\omega = 0.5$ respectively and $r_T = 3$; the trajectories (*1*) and (*2*) correspond to RR and LL strategies respectively; loci of the initial positions and the terminal zero range rate lines for LL and RR strategies are shown with *dashed and dashed-dotted lines* respectively. Dots on the terminal zero range rate lines show the terminal positions $r_T = 3$; (**a**) the encounter time for trajectories (*1*) and (*2*) is $T = \pi/5$ in *Fig. 3a* and $T = \pi/3$ in *Fig. 3b*; (**c**) the loci of the initial relative positions (circle shown with *bold solid line*) and trajectories (*fine solid lines*) for RL strategy with $\omega = 1.3$, $r_T = 1$. The circle of terminal relative positions is shown with *dotted line*. The values of the terminal relative bearing for RL trajectories are: *1*: $\phi_T = -\pi$; *2*: $\phi_T = -\pi/2$; *3*: $\phi_T = -\pi/3$; *4*: $\phi_T = -\pi/8$; *5*: $\phi_T = \pi/30$; *6*: $\phi_T = -12\pi/11$. The initial positions for the *1*st and *5*th trajectories bound the loci of the initial positions for the trajectories with decreasing relative distance, while trajectory *6* starts outside such loci

We can now define the loci of the initial relative positions $\Re_{LL}(\theta_0, \omega)$, $\Re_{RR}(\theta_0, \omega)$, $\Re_{RL}(\theta_0, \omega)$ and $\Re_{LR}(\theta_0, \omega)$ for LL, RR, RL and LR optimal strategies respectively as follows:

$$\Re_{LL}(\theta_0, \omega) \equiv \left\{(x_0, y_0, u) : (x_0, y_0) \in \bigcup_{r_T} \Re(r_T, \theta_0, \omega), u^T = (-1, -1)\right\},$$

$$\Re_{RR}(\theta_0, \omega) \equiv \left\{(x_0, y_0, u) : (x_0, y_0) \in \bigcup_{r_T} \Re(r_T, \theta_0, \omega), u^T = (1, 1)\right\},$$

$$\Re_{RL}(\theta_0, \omega) \equiv \left\{(x_0, y_0, u) : (x_0, y_0) \in \bigcup_{r_T} \Re(r_T, \theta_0, \omega), u^T = (1, -1)\right\},$$

$$\Re_{LR}(\theta_0, \omega) \equiv \left\{(x_0, y_0, u) : (x_0, y_0) \in \bigcup_{r_T} \Re(r_T, \theta_0, \omega), u^T = (-1, 1)\right\}.$$

5.3 Triple Point and Its Properties

A triple point is defined as a point on the plane of the initial relative positions of aircraft such that the three optimal strategies result in the same terminal miss distance. To find a triple point for $0 < \theta_0 < \pi$, one needs to find a point of intersection of the branch of the loci of initial position for the LL strategy (23), the branch of the loci of initial positions for RR strategy (24) and the loci of initial positions of the RL strategy (18). Thus, one needs to satisfy the conditions

$$\begin{aligned}
&x^{LL}(T_1^{tp})|_{\phi_T=\theta_T/2} = x^{RR}(T_2^{tp})|_{\phi_T=\theta_T/2-\pi},\\
&y^{LL}(T_1^{tp})|_{\phi_T=\theta_T/2} = y^{RR}(T_2^{tp})|_{\phi_T=\theta_T/2-\pi},\\
&x^{LL}(T_1^{tp})|_{\phi_T=\theta_T/2} = x^{RL}(r_T^{tp}, \phi_T^{tp}),\\
&y^{LL}(T_1^{TP})|_{\phi_T=\theta_T/2} = y^{RL}(r_T^{tp}, \phi_T^{tp})
\end{aligned} \tag{31}$$

where T_1^{tp} and T_2^{tp} are the times of the encounter for the LL and RR strategies at the triple point respectively, r_T^{tp} and ϕ_T^{tp} are the terminal miss distance and the terminal relative bearing at the triple point. Conditions (31) can be written as a system of four trigonometric equations,

$$\begin{aligned}
&r_T^{tp}\left[\sin((\theta_0 - \omega T_1^{tp} - T_1^{tp})/2) + \sin((\theta_0 + \omega T_2^{tp} + T_2^{tp})/2)\right]\\
&\quad + 2\cos\theta_0/\omega - 2 - \left[\cos(\theta_0 - \omega T_1^{tp}) + \cos(\theta_0 + \omega T_2^{tp})\right]/\omega\\
&\quad + \cos T_1^{tp} + \cos T_2^{tp} = 0,
\end{aligned} \tag{32}$$

$$\begin{aligned}
&r_T^{tp}\left[\cos((\theta_0 - \omega T_1^{tp} - T_1^{tp})/2) + \cos((\theta_0 + \omega T_2^{tp} + T_2^{tp})/2)\right]\\
&\quad - 2\sin\theta_0/\omega + \left[\sin(\theta_0 - \omega T_1^{tp}) + \sin(\theta_0 + \omega T_2^{tp})\right]/\omega\\
&\quad + \sin T_1^{tp} - \sin T_2^{tp} = 0,
\end{aligned} \tag{33}$$

$$r_T^{tp}\big[\sin((\theta_0-\omega T_1^{tp}-T_1^{tp})/2)-\sin(\phi_f^{tp}+\theta_0/(1+\omega))\big]$$
$$-\cos(\theta_0-\omega T_1^{tp})/\omega+(\omega+1)\cos(\theta_0/(1+\omega))/\omega$$
$$-2+\cos T_1^{tp}=0, \tag{34}$$
$$r_T^{tp}\big[\cos((\theta_0-\omega T_1^{tp}-T_1^{tp})/2)-\cos(\phi_f^{tp}+\theta_0/(1+\omega))\big]$$
$$+\sin(\theta_0-\omega T_1^{tp})/\omega-(\omega+1)\sin\big[\theta_0/(1+\omega)\big]/\omega$$
$$-2+\sin T_1^{tp}=0, \tag{35}$$

with the unknowns $(T_1^{tp}, T_2^{tp}, r_T^{tp}, \phi_T^{tp})$. The initial guesses for the unknowns can be obtained from the solution for the triple point for identical aircraft ($\omega=1$). In this case, $T_1=T_2$. Simple geometric considerations yield

$$T_1=T_2=\arccos\big\{2\sin(\theta_0/2)/[r_T+2\sin(\theta_0/2)]\big\}. \tag{36}$$

Also, for $\omega=1$ [5],

$$\phi_T=-\pi/2, \qquad r_T^{tp}=\frac{(1-\cos(\theta_0/2))^2}{\sin(\theta_0/2)+\cos(\theta_0/2)-1}. \tag{37}$$

The polar coordinates (r^{tp}, ϕ^{tp}) of the triple point are shown in Fig. 4 as functions of ω for different values of θ_0. One can see that the radial coordinate r of the triple

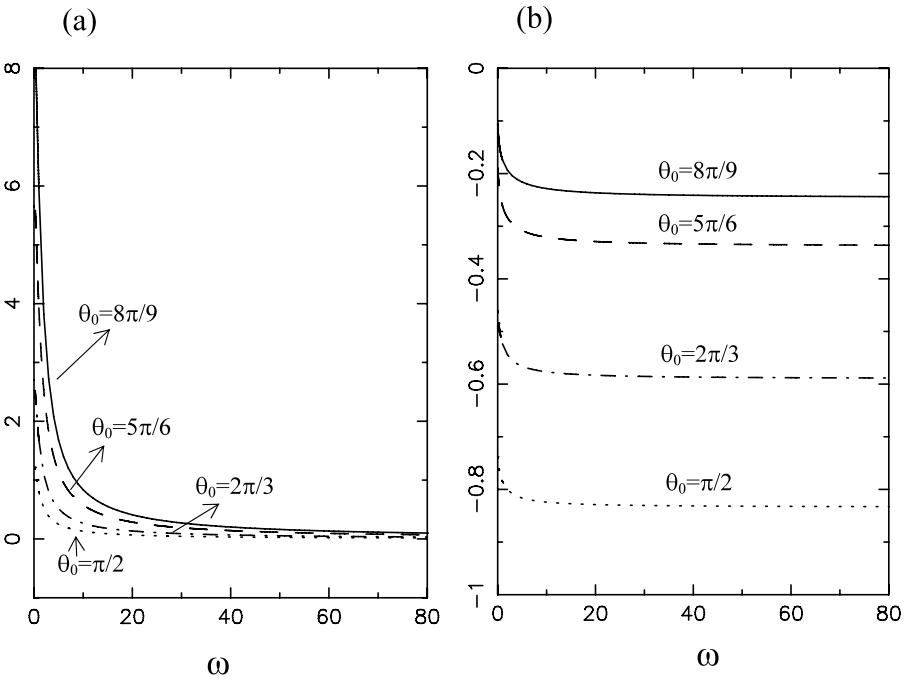

Fig. 4 Polar coordinates r (see (**a**)) and ϕ (see (**b**)) of a triple point as functions of ω for different θ_0

point decreases with increase in ω and asymptotically approaches zero, while the angular coordinate ϕ asymptotically approaches a constant value with increase in ω. Also, the radial coordinate increases as θ_0 approaches the value π.

5.4 Dispersal Curves

For a given θ_0 and r_T, consider the point on the plane of the initial relative positions (x_0, y_0) that serves as the initial condition for two different optimal strategies that result in the same terminal miss distance. Such point is called a dispersal point. A loci of the dispersal points is called a dispersal curve. Note that the dispersal curves also represent the switching curves, as crossing them would result in switching to different optimal strategy. Firstly, we consider the case $\theta_0 = \pi$ and prove the following property.

Property 5.7 *For $\theta_0 = \pi$, the RR-LL dispersal curve coincides with the y-axis.*

Proof It is straightforward to show that, for $\theta_0 = \pi$, the loci of initial conditions for the LL strategies, (23), and the loci of initial conditions for the RR strategies, (24), are symmetric relative to the y-axis and intersect at $x = 0$. It follows from (23) and (24) that, for a given T,

$$\begin{aligned} y^{LL}(T)|_{\phi_T=\theta_T/2} &= y^{RR}(T)|_{\phi_T=\theta_T/2-\pi} \\ &= r_T \sin((\omega T + T)/2) + \sin T + [\sin(\omega T)]/\omega, \end{aligned} \tag{38}$$

$$\begin{aligned} x^{LL}(T)|_{\phi_T=\theta_T/2} &= -x^{RR}(T)|_{\phi_T=\theta_T/2-\pi} \\ &= r_T \cos((\omega T + T)/2) + [\cos(\omega T) - 1]/\omega - (1 - \cos T). \end{aligned} \tag{39}$$

Therefore, these branches of loci are symmetric relative to the y-axis. Equation (39) shows that for any r_T the condition $x^{LL}(T)|_{\phi_T=\theta_T/2} = x^{RR}(T)|_{\phi_T=\theta_T/2-\pi}$ can only be satisfied if $r_T \cos((\omega T + T)/2) + [\cos(\omega T) - 1]/\omega - (1 - \cos T) = 0$. Therefore, the x-coordinate of the intersection is $x^{LL}(T)|_{\phi_T=\theta_T/2} = x^{RR}(T)|_{\phi_T=\theta_T/2-\pi} = 0$ and the RR-LL dispersal curve coincides with the y-axis. □

We now consider the RR-LL dispersal curves for any value of θ_0. To find the RR-LL dispersal point, one needs to find a point of intersection of the loci of initial position for the LL strategy (23) and of the loci of initial positions for the RR strategy (24). Thus, for a given r_T, one needs to find the times of the encounter T_1 and T_2 for the LL and RR strategies so that $x^{LL}(T_1)|_{\phi_T=\theta_T/2} = x^{RR}(T_2)|_{\phi_T=\theta_T/2-\pi}$, $y^{LL}(T_1)|_{\phi_T=\theta_T/2} = y^{RR}(T_2)|_{\phi_T=\theta_T/2-\pi}$. These conditions can be written as two trigonometric equations,

$$\begin{aligned} &r_T\big[\sin((\theta_0 - \omega T_1 - T_1)/2) + \sin((\theta_0 + \omega T_2 + T_2)/2)\big] \\ &\quad - \big[\cos(\theta_0 - \omega T_1) + \cos(\theta_0 + \omega T_2)\big]/\omega \\ &\quad + 2\cos\theta_0/\omega - 2 + \cos T_1 + \cos T_2 = 0, \end{aligned} \tag{40}$$

$$\begin{aligned} &r_T\big[\cos((\theta_0 - \omega T_1 - T_1)/2) + \cos((\theta_0 + \omega T_2 + T_2)/2)\big] \\ &\quad + \big[\sin(\theta_0 - \omega T_1) + \sin(\theta_0 + \omega T_2)\big]/\omega \\ &\quad - 2\sin\theta_0/\omega - 2 + \sin T_1 - \sin T_2 = 0. \end{aligned} \tag{41}$$

with unknowns (T_1, T_2). The initial guesses for T_1 and T_2 can be obtained from the solution for identical aircraft (36). To construct a dispersal curve, one needs to solve (40) and (41) incrementally for the value of r_T between 0 and r_T^{tp}.

Figure 5a shows the RR-LL dispersal curves for $\theta_0 = 2\pi/3$ and for several values of ω. The dispersal curves are plotted for the values of terminal miss distance between zero and the terminal miss distance at the triple point. The RR-LL dispersal curve for the case of identical aircraft is also shown for comparison with dotted line. One can see that the further the value of ω from unity (both smaller and larger than the unity), the larger the curvature of the dispersal curve. Also, with an increase in ω ($\omega > 1$), the dispersal curves move anticlockwise relative to the dispersal curve for identical aircraft, while with a decrease in ω ($\omega < 1$) the dispersal curves move clockwise with respect to the dispersal curve for identical aircraft.

Consider now the RL-LL and RL-RR dispersal curves. To find the RL-LL dispersal point, one needs to find a point of intersection of the loci of initial positions for the LL strategy (23) and the loci of initial positions for the RL strategy, that is $x^{LL}(T_1)|_{\phi_T=\theta_T/2} = x^{RL}(r_T, \phi_T)$, $y^{LL}(T_1)|_{\phi_T=\theta_T/2} = y^{RL}(r_T, \phi_T)$. These conditions can be written as two trigonometric equations,

$$r_T\big[\sin((\theta_0 - \omega T_1 - T)/2) - \sin(\phi_T + \theta_0/(1+\omega))\big] - \cos(\theta_0 - \omega T_1)/\omega + (1+\omega)\cos[\theta_0/(1+\omega)]/\omega - 2 + \cos T_1 = 0, \tag{42}$$

$$r_T\big[\cos((\theta_0 - \omega T_1 - T_1)/2) - \cos(\phi_T + \theta_0/(1+\omega))\big] + \sin(\theta_0 - \omega T_1)/\omega - (1+\omega)\sin[\theta_0/(1+\omega)]/\omega + \sin T_1 = 0, \tag{43}$$

with the unknowns (T_1, ϕ_T).

The RL-RR dispersal curve can be found in a similar way by solving two trigonometric equations,

$$-r_T\big[\sin((\theta_0 + \omega T_2 + T_2)/2) + \sin(\phi_T + \theta_0/(1+\omega))\big] + \cos(\theta_0 + \omega T_2)/\omega + (1+\omega)\cos[\theta_0/(1+\omega)]/\omega - 2\cos(\theta_0)/\omega - \cos T_2 = 0, \tag{44}$$

$$-r_T\big[\cos((\theta_0 + \omega T_2 + T_2)/2) + \cos(\phi_T + \theta_0/(1+\omega))\big] - \sin(\theta_0 + \omega T_2)/\omega - (1+\omega)\sin[\theta_0/(1+\omega)]/\omega + 2\sin(\theta_0)/\omega + \sin T_2 = 0, \tag{45}$$

with the unknowns (T_2, ϕ_T). The initial guesses for the unknowns (T_1, ϕ_T) and (T_2, ϕ_T) can be found from the solution for the triple point for a given θ_0 and ω. To calculate the dispersal curves, (42) and (43) for RL-LL dispersal curve and (44) and (45) for RL-RR dispersal curve need to be solved incrementally for r_T starting with the value of terminal miss distance at the triple point r_T^{tp}.

Figures 5b and 5c show the partitioning of the plane of the initial relative positions of the aircraft into the regions of initial positions for different optimal strategies for $\theta_0 = 2\pi/3$ and for the values of ω smaller than, and larger than, unity respectively. The partition for the case of identical aircraft is also shown in both figures for comparison with solid lines. Rather interestingly, while the triple point and the RR-LL dispersal curves change with the change in ω, the corresponding RR-RL and LL-RL dispersal curves remain nearly parallel with a change in ω.

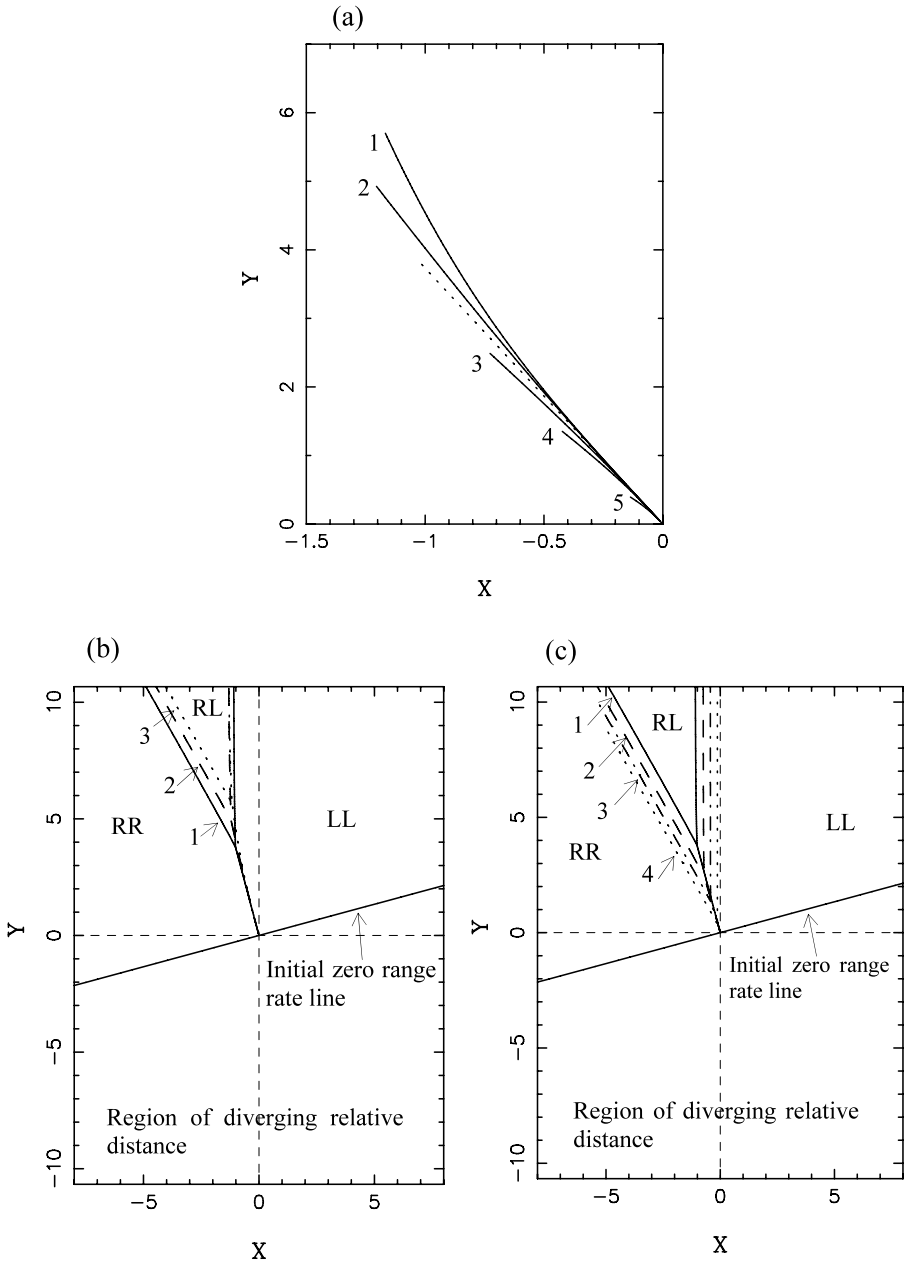

Fig. 5 Synthesis of optimal control diagrams for $\theta_0 = 5\pi/6$ and different ω; (**a**) RR-LL dispersal curves for $r_T \in [0, r_T^{tp}]$; *1*: $\omega = 0.1$; *2*: $\omega = 0.5$; *3*: $\omega = 2$; *4*: $\omega = 4$; *5*: $\omega = 15$; the dispersal curves for $\omega = 1$ are shown with *dotted lines*; *Figs. 5b* and *5c* show the partition of the plane of initial positions into the subregions of initial positions for different optimal strategies for different ω; (**b**) *1*: $\omega = 1$; *2*: $\omega = 0.5$; *3*: $\omega = 0.1$; (**c**) *1*: $\omega = 1$; *2*: $\omega = 2$; *3*: $\omega = 4$; *4*: $\omega = 15$

5.5 Properties of the Loci of Initial Positions for Different Optimal Strategies

For $\omega = 1$, the relative heading remains constant along the trajectories started on the loci $\Re_{LL}(\theta_0)$ and $\Re_{RR}(\theta_0)$, so these loci do not change along the optimal path. However, for the general case $\omega \neq 1$, the relative heading changes along the optimal trajectories and the loci $\Re_{LL}, \Re_{RR}$ become time-dependent, $\Re_{LL} = \Re_{LL}(\theta_0(t), \omega)$, $\Re_{RR} = \Re_{RR}(\theta_0(t), \omega)$. The relative heading also changes along the optimal RL and LR trajectories so that $\Re_{RL} = \Re_{RL}(\theta(t), \omega)$, $\Re_{LR} = \Re_{LR}(\theta(t), \omega)$.

It follows from the Properties 5.5 and 5.6 that, for the optimal trajectories started on the loci $\Re_{LL}(\theta_0, \omega)$ or $\Re_{RR}(\theta_0, \omega)$, a point on the trajectory will move towards the instantaneous zero range rate line. The instantaneous zero range rate line can move either towards this point or away from it for $\omega > 1$ and $\omega < 1$ respectively. In the former case, the rate of decrease of the relative distance of the trajectory point to the instantaneous zero range rate line is larger than the rate of change of the instantaneous zero range rate line. In the latter case, the rate of change of the distance of the point on the trajectory is larger than the rate of change of the instantaneous zero range rate line. Thus, the optimal trajectories started on the loci $\Re_{LL}(\theta_0, \omega)$ and $\Re_{RR}(\theta_0, \omega)$ stay within the loci where they started. For the optimal trajectories started on the loci $\Re_{LR}(\theta_0(t_0), \omega)$ or $\Re_{RL}(\theta_0(t_0), \omega)$, the relative heading decreases towards zero along the optimal path. Thus, as the time approaches the terminal time, the loci $\Re_{LR}(\theta(t), \omega)$ or $\Re_{RL}(\theta(t), \omega)$ expand and approach the half-plane described by condition (27). It can be shown that the optimal trajectory will stay within the expanding loci $\Re_{LR}(\theta(t), \omega)$ or $\Re_{RL}(\theta(t), \omega)$, if it started within the loci $\Re_{LR}(\theta_0(t_0), \omega)$ or $\Re_{RL}(\theta_0(t_0), \omega)$.

Thus, the optimal trajectory will never leave the loci of relative positions corresponding to a given optimal strategy. As a result, switching between the nonsingular controls is not optimal for the trajectory that starts within the loci of initial relative positions $\Re_{LL}(\theta_0, \omega)$, $\Re_{RR}(\theta_0, \omega)$, $\Re_{RL}(\theta_0, \omega)$ or $\Re_{LR}(\theta_0, \omega)$ and has a control strategy associated with the loci where it starts.

5.6 Singular Arcs

The results in the previous sections have been obtained assuming nonsingular controls. This section investigates the existence of singular arcs and the optimality of the corresponding trajectories.

We now consider the Hamiltonian in the Cartesian coordinate system. The switch functions are given by $\Phi_1^{(c)} = -\lambda_x y + \lambda_y x - \lambda_\theta$, $\Phi_2^{(c)} = \omega\lambda_\theta$.

Lemma 5.2 *The only possible singular arcs are those with the control function equal to zero* (*that is*, *one of aircraft flies a straight path*).

Proof The proof is identical to that in [5], as the switch functions and the adjoint variables are similar (apart from the positive factor ω) for the case of identical aircraft and the case of aircraft with different turn rate. □

Lemma 5.3 *The strategies that include zero control functions are suboptimal.*

Proof The proof is similar to that in [5], however is significantly more cumbersome. The outline is as follows. Consider a zero control trajectory that starts on the loci of the initial conditions for the optimal nonsingular strategy for a given r_T and θ_0, and calculate a point on the trajectory after the time interval Δt (selected so that $\omega \Delta t$ is small). It can be shown, by taking expansions in small $\omega \Delta t$, that after the time interval Δt the point on the zero control trajectory represents the initial relative position for the optimal nonsingular trajectory with the terminal miss distance smaller than r_T. Therefore zero control trajectory would result in smaller terminal miss distance compared with the optimal nonsingular trajectory starting at the same initial relative positions, and switching to the zero control strategy is suboptimal. □

5.7 Algorithms for Optimal Collision Avoidance Strategies

Analytic solutions for the extremals and the loci of the initial conditions developed in this paper, together with the analysis of the properties of the solutions, make the construction of the synthesis of optimal control a relatively simple task. To find the optimal cooperative collision avoidance strategy for a given θ_0 and ω, the plane of the initial relative positions (Fig. 1) needs to be partitioned into the two half-planes of diverging and converging relative distance. The half-plane of converging relative distances needs to be further partitioned into three subregions of initial relative positions for different optimal collision avoidance strategies, as shown in Figs. 5b, 5c. For $0 < \theta_0 < \pi$, the three possible optimal strategies are LL, RR and RL strategies; while for $\pi < \theta_0 < 2\pi$, the possible optimal strategies are LL, RR and LR strategies. To construct the synthesis of optimal control diagram, one needs to perform the following steps:

- identify the initial zero range rate line that partitions the plane of the initial relative position into half-planes of diverging and converging relative distance, using (28);
- calculate the triple point r_T^{tp} (the algorithm for its determination is presented in Sect. 5.3);
- construct the LL-RR dispersal curve for $r_T \in [0, r_T^{tp}]$ (the algorithm is presented in Sect. 5.4);
- construct the dispersal curves for $r_T > r_T^{tp}$. For $0 < \theta_0 < \pi$, one needs to construct the RL-RR and LL-RL curves, while for $\pi < \theta_0 < 2\pi$ the LR-RR and LR-LL dispersal curves need to be computed (the algorithms are presented in Sect. 5.4).

The algorithms for calculation of the triple point and dispersal curves are based on numerical solutions of systems of trigonometric equations. Once the synthesis of the optimal control diagram is constructed, the optimal collision avoidance strategy is defined by the position of the second aircraft. Figure 6 illustrates this for $\theta_0 = 5\pi/6$, $\omega = 2$. One can see that in this case the initial position of the second aircraft is in the region of optimal left-left (LL) strategy, and therefore the optimal collision avoidance strategy in this case is for both aircraft to turn left with maximum turning capability.

Once the optimal strategy is determined for a given initial relative position and relative heading, the optimal trajectory can be calculated. The steps involved are as follows:

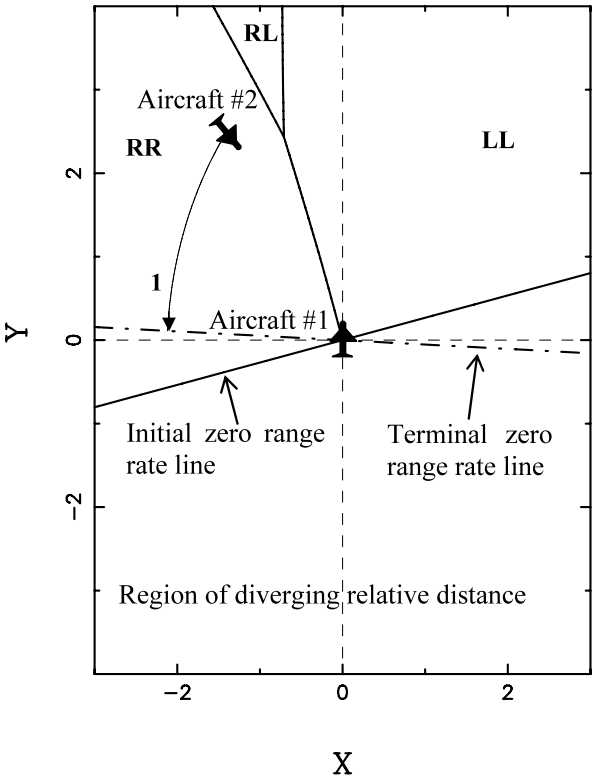

Fig. 6 Construction of the optimal collision avoidance strategy for a close proximity encounter, $\theta_0 = 5\pi/6$, $\omega = 2$: (*1*) is the optimal trajectory for RR strategy with $r_T = 2.12$, $T = 0.62$, the initial relative position of the second aircraft is $x_0 = -1.4$, $y_0 = 2.5$, $r_0 = 2.87$

RL and LR Strategies

- First, the time of the conflict T and the terminal miss distance r_T need to be found. T can be explicitly determined from the first of (17), while r_T is explicitly given by either (18) or (19), depending on the optimal strategy.
- The terminal relative bearing r_T can be determined explicitly by rewriting last two of (17) in the form

$$\tan(\phi_T + \sigma_1 T) = \frac{x_0 - \sigma_1\{1 + \cos[(1+\omega)T]/\omega + (1+\omega)\cos T/\omega\}}{y_0 - (1+\omega)\sin T/\omega + \sin[(1+\omega)T]/\omega}.$$

  The optimal trajectory can be computed using the last two of (16) by incrementally varying backward the time from zero to T.

RR and LL Strategies

- T and r_T can be found by numerically solving the system of two trigonometric equations (21) or (22).
- The terminal relative heading θ_T (and therefore the terminal relative bearing ϕ_T too) can be determined explicitly as

$$\theta_T = \theta_0 - \sigma_1(1-\omega)T.$$

- The optimal trajectory can be computed using last two of (20) by incrementally varying backward time from zero to T.

For RR and LL strategies, it may also be useful to plot the terminal zero range rate line using (29), as shown in Fig. 6.

The above steps need to be repeated once the updated information about the relative positions and orientations for the two aircraft becomes available. This type of process is routine in the architectural design of many flight management systems (FMS).

6 Discussion and Conclusions

The analysis presented in this paper reveals the structure of the synthesis of the optimal control solution for close proximity encounters of aircraft (ships) with unequal turn capabilities. The analysis shows that the optimal strategies are the combinations of limiting (maximum or minimum) values of control functions denoted by right-right (RR), right-left (RL), left-left (LL) and left-right (LR) strategies, as in the case of identical aircraft [3–5]. Also, the synthesis of the optimal control diagram (the partitioning of the plane of the initial relative positions into the subregions of the initial positions for different optimal strategies) has a common structure for any value of ω, that is characterized by the presence of the triple point and the three subregions of different optimal strategies for any given initial relative heading θ_0. However, the structure of the solution for $\omega \neq 1$ is significantly more complex. The loci of the initial conditions for the RR and LL strategies represent spirals, that are bounded and converging for increasing ω when $\omega > 1$, and are unbounded and diverging for decreasing ω when $\omega < 1$. Thus, Merz' solution for identical aircraft [3–5] represents a degenerate case when the spirals turn into circles. Compared to the solution for identical turning rates $\omega = 1$ [3–5], where the loci of initial conditions for the optimal RR and LL strategies remain unchanged along the optimal path, the regions of initial conditions for all optimal strategies change with time along the optimal path for the general case $\omega \neq 1$.

The paper presents simple algorithms for the computation of the synthesis of optimal control based on the solutions of the systems of trigonometric equations. The synthesis of the optimal control solution presented in this paper can be used as a benchmark (ideal) solution for setting and validating the air traffic rules, and also for validation of a significant subclass of behavior for more complicated automated air traffic control systems.

References

1. Fulton, N.L.: Regional airspace design: a structured systems engineering approach. Doctoral dissertation, University of New South Wales (11 December 2002)
2. Fulton, N.L.: Airspace design: towards a rigorous specification of conflict complexity based on computational geometry. Aeronaut. J., 75–84 (February 1999)
3. Merz, A.W.: Optimal aircraft collision avoidance. In: Proc. Joint Automatic Control Conf., Paper 15-3, pp. 449–454 (1973)

4. Merz, A.W.: Optimal evasive manoeuvres in maritime collision avoidance. Navigation **20**(2), 144–152 (1973)
5. Tarnopolskaya, T., Fulton, N.: Optimal cooperative collision avoidance strategy for coplanar encounter: Merz's solution revisited. J. Optim. Theory Appl. **140**(2), 355–375 (2009)
6. Miele, A., Wang, T., Chao, C.S., Dabney, J.B.: Optimal control of a ship for collision avoidance maneuvers. J. Optim. Theory Appl. **103**(3), 495–518 (1999)
7. Miele, A., Wang, T.: Optimal trajectories and guidance schemes for ship collision avoidance. J. Optim. Theory Appl. **129**(1), 1–20 (2006)
8. Krozel, J., Peters, M.: Conflict detection and resolution for free flight. Air Traffic Contr. Q. **5**(3), 181–211 (1997)
9. Miele, A., Wang, T., Chao, C.S., Dabney, J.B.: Optimal control of a ship for course change and sidestep maneuvers. J. Optim. Theory Appl. **103**(2), 259–282 (1999)
10. Miloh, T., Pachter, M.: Ship collision-avoidance and persuit-evasion differential games with speed-loss in a turn. Comput. Math. Appl. **18**(1–3), 77–100 (1989)
11. Krozel, J., Mueller, T., Hunter, G.: Free flight conflict detection and resolution analysis. In: AIAA Guidance, Navigation, and Control Conf., Paper 96-3763, pp. 1–11 (1996)
12. Clements, J.C.: The optimal control of collision avoidance trajectories in air traffic management. Transp. Res. Part B **33**, 265–280 (1999)
13. Clements, J.C.: Optimal simultaneous pairwise conflict resolution maneuvers in air traffic management. J. Guid. Control Dyn. **25**(4), 815–818 (2002)
14. Menon, P.K., Sweriduk, G.D., Sridhar, B.: Optimal strategies for free-flight air traffic conflict resolution. J. Guid. Control Dyn. **22**(2), 202–211 (1999)
15. Raghunathan, A.U., Gopal, V., Subramanian, D., Biegler, L.T., Samad, T.: Dynamic optimization strategies for three-dimensional conflict resolution of multiple aircraft. J. Guid. Control Dyn. **27**(4), 586–594 (2004)
16. Hu, J., Prandini, M., Sastry, S.: Optimal coordinated maneuvers for three-dimensional aircraft conflict resolution. J. Guid. Control Dyn. **25**(5), 888–900 (2002)
17. Paielli, R.: Modeling maneuver dynamics in air traffic conflict resolution. J. Guid. Control Dyn. **26**(3), 407–415 (2003)
18. Durand, N.: Optimisation de Trajectoires pour la Resolution de Conflits en Route. PhD Dissertation, Institut National Polytechnique de Toulouse (28 May 1996)
19. Emery, S.: Design aeronautical study for Broome international airport terminal airspace (14 March 2004)
20. Shukla, U.S., Mahapatra, P.R.: The proportional navigation dilemma—pure or true? IEEE Trans. Aerosp. Electron. Syst. **26**(2), 382–392 (1990)
21. Goodchild, C., Vilaplana, M., Elefante, S.: Co-operative optimal airborne separation assurance in free flight airspace. In: Proc. 3rd USA/Europe Air Traffic Management R&D Seminar, Napoli, 13–16 June 2000
22. Christodoulou, M.: Automatic commercial aircraft-collision avoidance in free flight: the three-dimensional problem. IEEE Trans. Intell. Transp. Syst. **7**(2), 242–249 (2006)
23. Cesarone, J., Eman, K.F.: Efficient manipulator collision avoidance by dynamic programming. Robot. Comput. Integr. Manuf. **8**(1), 35–44 (1991)
24. Tomlin, C., Pappas, G.J.: Conflict resolution for air traffic management: a study in multiagent hybrid systems. IEEE Trans. Automat. Contr. **43**(4), 509–521 (1998)
25. Bicchi, A., Pallotino, L.: On optimal cooperative conflict resolution for air traffic management systems. IEEE Trans. Intell. Transp. Syst. **1**(4), 221–232 (2000)
26. Mitchell, I.M., Bayen, A.M., Tomlin, C.J.: A time-dependent Hamilton-Jocobi formulation of reachable sets for continuous dynamic games. IEEE Trans. Automat. Contr. **50**(7), 947–957 (2005)
27. Mitchell, I.M., Tomlin, C.J.: Overapproximating reachable sets by Hamilton-Jacobi projections. J. Sci. Comput. **19**(1–3), 323–346 (2003)
28. International Civil Aviation Organization: Annex 2, Rules of the Air. Chapter 3, ninth ed. Amendment 36. Montreal, Canada (November 2001)
29. Pontryagin, L.S., Boltyanski, W.G., Gamkrelidze, R.V., Mishchenko, E.F.: The Mathematical Theory of Optimal Processes. Wiley, New York (1965)
30. Bryson, A.E.: Dynamic Optimization. Addison-Wesley, Reading (1999)
31. Fleming, W.H., Rishel, R.W.: Deterministic and Stochastic Optimal Control. Springer, Berlin (1975)